An Engineered Human Fc Domain that Behaves like a pH-Toggle Switch for Ultra-Long Circulation Persistence

Tae Hyun Kang, Chang-Han Lee, Tae Hyun Kang, Ophélie Godon, Makiko Watanabe, George Delidakis, Caitlin Gillis, Delphine Sterlin, David Hardy, Michel Cogné, et al.

An Engineered Human Fc Domain that Behaves like a pH-Toggle Switch for Ultra-Long Circulation Persistence

Chang-Han Lee[1,†], Tae Hyun Kang[1,#,†], Ophélie Godon[2], Makiko Watanabe[1], George Delidakis[1], Caitlin M. Gillis[2], Delphine Sterlin[2], David Hardy[3], Michel Cogné[4], Lynn E. Macdonald[5], Andrew J. Murphy[5], Naxin Tu[5], Jiwon Lee[6], Jonathan R. McDaniel[1], Emily Makowski[7], Peter M. Tessier[7,8,9], Aaron S. Meyer[10], Pierre Bruhns[2,*], and George Georgiou[1,11,12 *]

Author affiliations

1 Department of Chemical Engineering, University of Texas at Austin, Austin, TX, USA.

2 Unit of Antibodies in Therapy and Pathology, Institut Pasteur, UMR1222 INSERM, F-75015 Paris, France

3 Experimental Neuropathology Unit, Infection and Epidemiology Department, Institut Pasteur, 25, rue du Docteur Roux, 75015, Paris, France

4 Limoges University, Limoges, France

5 Regeneron Pharmaceuticals, Inc., Tarrytown, NY, USA.

6 Thayer School of Engineering, Dartmouth College, Hanover, NH, USA

7 Departments of Pharmaceutical Sciences, University of Michigan, Ann Arbor, MI, USA

8 Departments of Chemical Engineering, University of Michigan, Ann Arbor, MI, USA

9 Departments of Biomedical Engineering, University of Michigan, Ann Arbor, MI, USA

10 Department of Bioengineering, University of California at Los Angeles, Los Angeles, CA, USA.

11 Department of Molecular Bioscience, University of Texas at Austin, Austin, TX, USA.

12 Department of Biomedical Engineering, University of Texas at Austin, Austin, TX, USA.

Current address: Department of Applied Chemistry, Kookmin University, Seoul, Republic of Korea

† These authors contributed equally.

*These authors jointly supervised this work. To whom correspondence should be addressed. E-mail: gg@che.utexas.edu; Telephone: 512-471-6975; Fax: 512-471-7963. bruhns@pasteur.fr; Telephone: +33145688629.

Abstract

The pharmacokinetic properties of antibodies are largely dictated by the pH-dependent binding of the IgG fragment crystallizable (Fc) domain to the human neonatal Fc receptor (hFcRn). Engineered Fc domains that confer a longer circulation half-life by virtue of more favorable pH-dependent binding to hFcRn are of great therapeutic interest. Here we developed a pH Toggle switch Fc variant containing the L309D/Q311H/N434S (DHS) substitutions, which exhibits markedly improved pharmacokinetics relative to both native IgG1 and widely used half-life extension variants, both in conventional hFcRn transgenic mice and in new knock-in mouse strains. engineered specifically to recapitulate all the key processes relevant to human antibody persistence in circulation, namely: (i) physiological expression of hFcRn, (ii) the impact of hFcγRs on antibody clearance and (iii) the role of competing endogenous IgG. DHS-IgG retains intact effector functions, which are important for the clearance of target pathogenic cells and also has favorable developability.

Introduction

IgG isotype antibodies avoid clearance by endolysosomal degradation by virtue of their pH-dependent binding to the neonatal Fc receptor (FcRn), which is expressed by cells in nearly every organ in mammals[1–3]. The FcRn receptor consists of the glycosylated heavy α-chain polypeptide, an MHC I class family member which associates with β2-microglobulin (β2m)[4,5]. IgG internalized by pinocytosis binds to FcRn at endosomal pH (5.5-6.0) and as a result, instead of being directed to the endolysosomal compartment for degradation, IgG:FcRn complexes are sorted into tubules originating from sorting endosomes and directed to return to the plasma membrane. Upon fusion with the plasma membrane, the intracellular fluid within the tubules is released and rapidly equilibrates with the extracellular pH 7.4[6–8]. At extracellular pH, the affinity of FcRn for the Fc domain is so low that antibodies are released back into circulation. This process occurs readily, despite the strong avidity effects of both the high local concentration of FcRn at the site of vesicle fusion, and the 2:1 stoichiometric binding of FcRn to IgG[9,10]. Biophysical studies have elucidated the molecular details of the IgG:FcRn interaction including the role of residues in the CH2-CH3 interface of the Fc domain in contact with FcRn, the pivotal role of His310 and His435 on pH-dependent binding, and the significance of protein dynamics[11–13].

Engineering the human Fc domain to improve pharmacokinetic (PK) properties, (manifest as an increased area under the plasma drug concentration-time curve (AUC), a lower clearance rate and a longer β phase $T_{1/2}$[14,15]) is of great interest for therapeutic purposes[3,16–20]. Better pharmacokinetics enable less frequent administration and lower dosing, which in turn translate into improved patient compliance and lower costs. Mutations of the Fc domain that enhance the affinity for FcRn at both the endosomal and physiological pH have been shown to result in greater antibody clearance. In contrast, Fc mutations that

preferentially enhance FcRn affinity at pH 5.8 confer increased antibody half-life in circulation[16,18,20–23]. Fc domains containing the amino acid substitutions M428L/N434S (LS mutant), M252Y/S254T/T256E (YTE mutant), or H433K/N434F (KF mutant) confer 10- to 12-fold higher affinity for FcRn at pH 5.8, result in the greatest reported increase in antibody half-life (2- to 4- fold in circulation) in mice and in non-human primates, and are currently being evaluated in multiple clinical trials[16,24–26]. Notably, ravulizumab, a complement C5-inhibiting antibody containing the LS mutations, was FDA-approved for paroxysmal nocturnal hemoglobinuria and shown to have a serum half-life of ~49.7 days[27], and MEDI8897, a respiratory syncytial virus (RSV)-neutralizing antibody containing the YTE mutations, was shown to have a serum half-life of ~70 days, compared to approximately 20 days for wild type (wt) IgG1, in infants in a phase 1b/2a study for prophylaxis against RSV infection[28].

While further improvements in human antibody pharmacokinetics are highly desirable, extensive protein engineering campaigns focused on identifying mutations that confer even higher affinity for FcRn at pH 5.8 relative to the YTE or LS Fc variants have so far failed to yield amino acid combinations capable of imparting even longer circulation half-life in animal models[20,23,29–31]. Notably, YTE- and LS- Fc domains have significant binding to FcRn at pH 7.4 under high avidity conditions[11]. Residual binding at pH 7.4 may have a negative effect on plasma recycling and circulation persistence[32,33]. Another key consideration in the engineering of antibodies with ultra-long circulation half-life is that any mutation introduced into the Fc domain, should not negatively impact other antibody characteristics such as effector functions or manufacturability[34]. For example, the YTE, LS and KF mutations reduce FcγR binding and effector functions to various degrees (depending

on the mutant antibody and patient FcγR allotype), and the YTE mutations have been reported to also reduce complement dependent cytotoxicity (CDC)[18,35].

Antibody pharmacokinetics are routinely evaluated in transgenic (Tg) mice overexpressing human FcRn (hFcRn) from non-native promoters[36,37]. However, the currently available hFcRn Tg mouse models do not recapitulate many of the mechanisms that affect antibody clearance. Key limitations of the existing mouse models used for antibody pharmacokinetic studies arise from: (i) non-physiological levels of transgene hFcRn expression relative to mouse FcRn in wild-type animals[38]; (ii) expression of mouse β2m instead of human β2m (hβ2m) in many of the currently used models [36,37,39]; (iii) absence of endogenously produced human IgG to compete for hFcRn binding[40]; and (iv) no ability to account for the effect of binding to human FcγRs in clearance[41,42]. To address these limitations, as part of this work we constructed new knock-in mouse models that express hFcRn, hβ2m, and hFcγRs; and, in addition, produce endogenously chimeric mouse-human IgG1, composed of mouse variable regions and human constant regions for the heavy and light chain (hIgG1,κ).

Here, we report the engineering of a human IgG Fc domain which, by virtue of having moderately higher affinity for FcRn at pH 5.8 but no detectable binding at pH 7.4 under high avidity conditions, confers improved antibody PK properties compared to the clinical stage YTE and LS variants, both in the commonly used $hFcRn^{Tg}$ mouse model (hemizygotic 276) as well as in our new knock-in model (hFcRn-hβ2m-hFcγRs-hIgG1,κ mice). Importantly, we show that antibodies utilizing our engineered ultra-long half-life Fc domain display the full range of effector functions as the wt Fc domain while exhibiting far favorable biophysical properties for clinical development.

Results

Pharmacokinetics properties of an engineered human Fc variant: We developed a strategy that capitalizes on *E.coli* display of large combinatorial IgG libraries (Anchored Periplasmic Expression (APEx) technology[43–46]) for the isolation of clones expressing human IgG1 with mutated Fc domains that bind selectively to the human FcRn/human β2m complex (hFcRn:hβ2m) at pH 5.8 but not at pH 7.4 (**Fig. 1a**). Select regions of the human IgG1 C_H2-C_H3 hinge were combinatorially mutagenized (**Supplementary Fig. 1a-c** and **Supplementary Table 1**) to create a library of $>10^8$ transformants. Briefly, *E. coli* spheroplasts expressing mutated human IgG1 (Trastuzumab) anchored on the external leaflet of the inner membrane were first screened by FACS for binding to Alexa488-labelled hFcRn:hβ2m. Three rounds of FACS with hFcRn:hβ2m at pH 5.8 were performed to enrich antibodies with Fc domains with higher binding affinity at pH 5.8. The pool of clones enriched for enhanced binding at endosomal pH was then subjected to a competitive, two-step labeling process to eliminate variants that have detectable binding at pH 7.4 to high avidity, dimeric, GST-hFcRn:hβ2m. For this purpose, spheroplasted cells were labelled with an excess of Alexa647-labeled GST-hFcRn:hβ2m (red) at pH 7.4 and then spheroplasts were washed with pH 7.4 PBS. The spheroplasts were subsequently labelled with monomeric hFcRn:hβ2m-Alexa488 (green) at pH 5.8, and clones with high green fluorescence and low red fluorescence (i.e. absence of residual Alexa647-labeled GST-hFcRn:hβ2m from the first labeling step) were isolated and characterized (**Fig. 1a**). Four clones expressing different Fc variants from the last round of screening were isolated, individually confirmed to display pH-dependent binding by FACS and were all found to share three amino acid substitutions: V264E, L309D, and Q311H (EDH) (**Supplementary Fig. 1d**).

The four isolated antibody variants were produced in HEK293 cells. One variant, EDHY-IgG1 (V264E, L309D, Q311H, and N434Y) had a ~20-fold better affinity ($K_{D, pH5.8}$ = 28 nM) for hFcRn at pH 5.8 compared to wt IgG1 ($K_{D, pH5.8}$ = 550 nM) but also had residual binding at pH 7.4. A second variant, EDHS-IgG1 (V264E, L309D, Q311H, and N434S) had a ~6-fold increased affinity at 5.8 ($K_{D, pH5.8}$ =93 nM) but no apparent binding at pH 7.4 (**Supplementary Fig. 1e-g**). Very extensive mutagenesis efforts aimed at identifying mutations conferring even better $K_{D, \text{pH } 5.8}$ were unsuccessful, as all of the mutants isolated based on higher affinity at pH 5.8 had detectable binding at pH 7.4 based on FACS analysis.

Antibodies with the EDHS mutations in the Fc had drastically reduced binding to effector hFcγRs (**Supplementary Fig. 1h**); which was found to be due to the V264E mutation[47]. Since a V264E substitution has a minimal effect on hFcRn binding at pH 5.8[48], it was reverted back to a valine to yield the L309D/Q311H/N434S (DHS) Fc domain, resulting in complete recovery of hFcγR binding (**Supplementary Fig. 1h**). Moreover, these three amino acids substitutions did not affect the N-glycosylation pattern of the Fc domain which was comparable to that of wt IgG1 antibodies (**Supplementary Fig. 2**).

We performed a detailed analysis of the hFcRn:hβ2m binding kinetics of DHS antibodies as a function of pH using SPR analysis with immobilized hFcRn:hβ2m at low, medium or high density[11] (500, 2,000 or 4,000 RUs, **Fig. 1b-d** and **Supplementary Fig. 3**). Consistent with earlier reports[49], YTE- and LS-IgG1 showed moderate and significant binding, at pH 7.4, respectively when SPR analysis was performed with medium or high hFcRn:hβ2m densities (**Fig. 1b-c** and **Table 1**). In contrast, we could detect no binding of DHS- or wt-IgG1 to hFcRn:hβ2m at physiological conditions at even the highest density tested (**Fig. 1b**).

The pharmacokinetics of Trastuzumab, which does not bind any mouse targets, formatted with DHS-, YTE-, LS- or wt-IgG1 Fc domains were first evaluated in hemizygous hFcRn^{Tg} mice (hemizygotic Tg276), a widely used Tg mouse model for comparing the circulation persistence of human antibodies[37]. Following administration of a single intravenous dose (i.v. 2 mg/kg) by tail vein injection, the β phase $T_{1/2}$ (β phase half-life) of DHS was 2.0- and 3.1-fold higher compared to YTE and LS variants (290.9 ± 25.6 h compared to 148.4 ± 36.8 h and 92.9 ± 6.1 h, respectively, data are presented as mean ± standard deviation). Total drug exposure over time for DHS-IgG1 (AUC_{inf}) was 1.6-, 1.9- and 5.3-fold greater relative to YTE-, LS- and wt-IgG1 variants, respectively (**Fig. 1d** and **Table 2**). Antibody clearance followed biphasic kinetics, with a clearance rate of 0.11 ± 0.01 ml/day/kg for DHS-IgG1, approximately 6-fold lower than wt IgG1, and 1.9- and 2.2-fold lower than YTE- and LS-IgG1. Introduction of the DHS mutations into the Fc domain of IgG2, IgG3 (G3m16 allotype with H435 residue) or IgG4 subclasses also resulted in no detectable interaction with FcRn at pH 7.4, and likewise, conferred significantly improved pharmacokinetics for all the other three IgG subclasses (**Fig. 1e-g, Supplementary Fig. 4,** and **Supplementary Table 2**). Collectively, our data: (a) reveal that the DHS Fc domain imparts improved antibody PK properties in the hemizygous Tg276 hFcRn^{Tg} model relative to the best in class clinical stage, half-life extension variants YTE and LS and (b) support the hypothesis[32,33] that residual binding to FcRn at physiological pH has a major detrimental effect on antibody circulation persistence.

Pharmacokinetic studies in novel knock-in mouse models: To more accurately evaluate antibody pharmacokinetics we constructed knock-in (KI) mouse models that account for multiple processes known to affect human IgG clearance and homeostasis (**Fig. 2a-e**). In these KI mouse strains: (i) the hFcRn:hβ2m complex is expressed in a manner that faithfully

reflects mouse FcRn levels, (ii) the human effector FcγR family is expressed to account for FcγR-dependent clearance and finally, (iii) human IgG1, which, unlike murine IgG, competes with administered therapeutic antibodies for hFcRn binding[40], is produced endogenously. We developed a mouse in which the murine FcγR genes had been exchanged with the corresponding human genes, including introns and regulatory elements for *FCGR1A* and for *FCGR2A, FCGR2B, FCGR2C, FCGR3A*, and *FCGR3B* genes (hFcγR^{KI} mouse, intercross of VG6074 and VG1543 mice[50], **Fig. 2a-b**)[51]. The *Fcgrt* (mouse FcRn gene) was replaced with *FCGRT* (human FcRn gene, VG1481, **Fig. 2c**) and the *B2m* (mouse β2m gene) was replaced with *B2M* (human β2m gene, VG5153, **Fig. 2d**). The hFcRn^{KI} hβ2m^{KI} hFcγR^{KI} mice (designated as Marlene mice) were bred by crossing the four transgenes as shown in **Fig. 2e**. Finally, to account for the fact that endogenous mouse IgG does not compete with human IgG for binding to human FcRn[52], the heavy-chain constant region of human IgG1 (*IGHG1*) was knocked-in to replace the switch μ region of the mouse heavy-chain locus, and the human kappa light-chain constant region (*IGK*) was knocked-in to replace the mouse kappa light-chain region (kappa light chains are used in 95% of circulating antibodies in mice), thereby generating mice that exclusively produce human IgG1 heavy chains, predominantly associated to human kappa light chains (**Fig. 2f-g**). The hFcRn^{KI} hβ2m^{KI} hFcγR^{KI} hIgG1,κ^{KI} mice (designated as Scarlett mice) were bred by crossing the Marlene and the hIgG1,κ^{KI} mice (**Fig. 2h**). hFcRn expression was confirmed by immune-histochemistry and RT-PCR of spleens of Scarlett mice (**Fig. 2i** and **Supplementary Fig. 5**). Cell type-specific expression of hFcγRs in Marlene and Scarlett is reported in **Fig. 2j** and **Supplementary Fig. 6 is** similar to that of humans, and consistent with our earlier reported expression pattern for hFcγR^{KI} mice[50]. Scarlett mice displayed 440 ± 120 μg/mL of human IgG1 in serum and undetectable

levels of mouse IgG. The mouse IgG serum concentration in control C57BL/6J mice was 605 ± 147 μg/mL, in the same order of magnitude as human IgG1 in Scarlett mice.

We observed very comparable β-phase elimination half-life in the KI animals that produce endogenous human antibodies (Scarlett) for three different approved IgG1 antibodies (Trastuzumab, Rituximab, or Omalizumab) after a single intravenous dose (i.v. 2 mg/kg) by tail vein injection. Specifically, for Trastuzumab we compared the pharmacokinetics between the Scarlett mice and animals that do not have circulating human IgG1 (Marlene mice; **Supplementary Fig. 7**). The β-phase elimination half-life was 40% lower in the Scarlett mice underscoring how competition for FcRn binding by circulating human IgG1 impacts the pharmacokinetics of administered antibodies in $hFcRn^{Tg}$ mice.

Consistent with the trends observed in the hemizygous Tg276 $hFcRn^{Tg}$ mouse model, the data in **Fig. 2k** and **Table 3** reveal that in Scarlett mice - DHS antibodies have ≥ 50% longer β phase half-life ($P \leq 0.0001$ to LS- or YTE-IgG1), a proportional increase in AUC_{inf} ($P \leq 0.0001$ to LS- or YTE-IgG1), and a proportional decrease in clearance rate ($P \leq 0.0001$ to LS- or YTE-IgG1) relative to the YTE and LS variants. Compared to wt IgG1, the DHS mutations resulted in 4-fold longer β phase half-life and 5-fold greater AUC_{inf}.

Effector Functions and Biophysical Properties of DHS-Fc: Mutations that favorably impact antibody serum half-life can adversely affect binding to effector hFcγRs, in turn impairing the clearance of target cells by ADCC or ADCP[35]. Consistent with earlier reports, SPR measurements showed that the YTE mutations reduce binding to the low affinity FcγRs (i.e. hFcγRIIa, hFcγRIIb, hFcγRIIIa) by more than 3-fold. The LS substitutions have a more modest effect on hFcγR binding, resulting in a 2-fold reduction in affinity for hFcγRI and $hFc\gamma RIIa_{H131}$, and 3-fold reduction for $hFc\gamma RIIIa_{V158}$. In contrast, the affinities of the

DHS-IgG1 for hFcγRs were statistically indistinguishable (or slightly improved in the case of hFcγRIIIa$_{F158}$) compared to those of wt-IgG1 (**Table 4** and **Supplementary Fig. 8a**). Class-switched IgG2, IgG3 or IgG4 variants of Trastuzumab bearing DHS mutations also showed statistically indistinguishable binding to hFcγRs relative to their wt counterparts (**Supplementary Fig. 8b**). Not surprisingly, the *in vitro* ADCC activity of DHS-Trastuzumab IgG1 was identical to that observed with wt Trastuzumab in hFcγRIIIa-*V/V* and -*V/F* donors, but greater than that of YTE-Trastuzumab IgG1 or LS-Trastuzumab IgG1 (**Fig. 3a**). On the other hand, as expected[35], with homozygotic hFcγRIIIa-*F/F* donors, DHS-Trastuzumab IgG1 showed equivalent ADCC activities with wt Trastuzumab or LS-Trastuzumab IgG1 (**Fig. 3a**).

Next, we examined the ability of anti-CD20 (Rituximab) antibody variants to activate the classical complement pathway via the recruitment of C1q. Target cells ($CD20^+$ Raji) opsonized with DHS-Rituximab IgG1 antibodies had a higher level of cell surface-deposed C1q relative to wt-, LS- or YTE-Rituximab antibodies. DHS-Rituximab displayed 2-fold more potent CDC (0.7 ± 0.1 μg/ml) than wt- (1.5 ± 0.1 μg/ml) or LS-Rituximab (1.9 ± 0.1 μg/ml), and 10-fold more potent CDC than YTE-Rituximab, the latter which has already been reported to display significantly lower CDC activity than wt-Rituximab[18,48] (**Fig. 3b-c**).

Rheumatoid factor (RF) refers to auto-antibodies that bind to the Fc domain of immunoglobulins. The binding of RF to therapeutic antibodies is associated with faster clearance and increased antigen presentation and anti-drug antibodies[53–56]. We measured the RF binding of the wt-, DHS-, YTE- and LS-IgG1 by ELISA using polyclonal sera from donors with high RF titers. DHS-IgG1 showed binding to RF sera that was indistinguishable from that of wt-IgG1 and significantly lower than that observed with YTE-IgG1 and especially with LS-IgG1 (**Fig. 3d**).

Size exclusion chromatography (SEC) showed that for all 4 IgG subclasses, introduction of the DHS mutations did not affect protein solubility, nor did it lead to soluble aggregate formation (**Supplementary Fig. 9a**). The thermodynamic stability of therapeutic antibodies is one of the most important biophysical properties for clinical development [34,57,58]. The melting temperature (Tm) was comparable for the wt, DHS, and LS[35] Fc variants (**Table 5**) but was more than 6^{o}C lower for the YTE variant (**Table 5**)[34]. The susceptibility of the antibody variants to aggregation at 70°C was very high for YTE-IgG1, leading to visible precipitates within minutes, intermediate for LS-IgG1 and minimal for wt- and DHS-IgG1 (**Supplementary Fig. 9b-e**). Similarly, the YTE- and LS- IgG1 formed higher levels of soluble aggregates upon prolonged incubation at 50 ^{o}C (**Fig. 3e**). Finally, the self-association propensity of the various engineered Fc antibodies at room temperature was determined by affinity-capture self-interaction nanoparticle spectroscopy (AC-SINS) a widely used assay for antibody developability[58–60]. Earlier AC-SINS analyses using 137 FDA-approved antibody drugs, found that AC-SINS plasmon shifts >11.8 nm correspond to antibodies with high levels of self-association and which represents a development risk[58]. For DHS-IgG1 the AC-SINS plasmon shift was only 0.1 ± 0.5 nm; of note, YTE- and LS- antibodies also showed low plasmon shift in this assay albeit higher than that of DHS-IgG1 (**Fig. 3f**).

DISCUSSION

An ideal Fc domain for therapeutic applications must confer optimal pH dependent binding to hFcRn to achieve very long circulation half-life, maintain intact effector functions and display favorable biophysical properties suitable for clinical development[57,58]. To enable maximal antibody circulation half-life, an Fc domain should resemble a pH toggle switch with a low FcRn $K_{D\ \mathrm{pH\ 5.8}}$ and no detectable binding activity at pH 7.4. However, despite extensive efforts, engineering Fc domains with a lower FcRn $K_{D\ \mathrm{pH\ 5.8}}$ and no detectable binding at pH 7.4 under high avidity conditions had proven elusive[11,20]. Here, we used a two-step high-throughput screening strategy to isolate the DHS Fc variant, which has a 5-fold lower $K_{D\ \mathrm{pH\ 5.8}}$ for FcRn relative to wt-IgG1 Fc and no detectable binding at pH 7.4. Unlike antibodies containing the YTE or LS half-life extension mutations, the DHS Fc domain does not bind to high densities of immobilized hFcRn at pH 7.4 (**Fig. 1b-c** and **Table 1**). We found that, by virtue of the lack of detectable binding at pH 7.4 and despite having a lower affinity for FcRn at endosomal pH relative to the LS or YTE variants, DHS antibodies exhibit even more favorable pharmacokinetics in multiple mouse models. Specifically, as shown in **Fig. 1d** and **Table 2**, the DHS Fc domain confers significantly improved antibody pharmacokinetic properties relative to the YTE and LS variants in hemizygous Tg276 mice, a widely used model for antibody PK studies[37]. In the Tg276 model, hFcRn is transcribed from the CAG promoter, resulting in ubiquitous high-level gene expression[36]. A second transgenic mouse line, Tg32, in which hFcRn is under the control of the human hFcRn promoter, is also commonly used for antibody PK studies[46]; however, in this model the transgene is inserted in close proximity to a mouse enhancer region which in turn impacts transcription and tissue-specific expression. Because neither model fully recapitulates mouse endogenous FcRn expression[38], we constructed new models in which hFcRn and hβ2m are expressed from the

300 respective mouse promoters. The binding of antibodies to FcγRs, and in particular to FcγRs
301 expressed by liver-resident cells are known to affect antibody clearance[41,42]. However, since
302 human antibodies bind to mouse FcγRs with very different affinities than those of their
303 human counterparts[61,62] the effect of FcγR-mediated clearance of human IgG cannot be
304 properly accounted for in animals expressing murine IgG receptors. To address this
305 shortcoming, we further engineered hFcRn^{KI} hβ2m^{KI} mice to also express all the human FcγR
306 family proteins (Marlene mice). Yet another factor that plays an important role for
307 therapeutic antibody pharmacokinetics is the competition for hFcRn binding by endogenous,
308 circulating human IgG. Because mouse IgG does not bind to hFcRn[40] in some earlier
309 antibody PK studies in Tg276 or Tg32 hFcRn^{Tg} mice intravenous co-administration of IgG
310 (IVIG) was attempted as a surrogate for endogenous IgG competition. However, the effect of
311 IVIG was reported to be dependent on the mouse model and was more pronounced in animals
312 expressing lower hFcRn levels[40,63]. To overcome these problems, we further engineered the
313 Marlene mice to express chimeric mouse-human IgG1 containing the constant regions of
314 human IgG1 heavy chain and human kappa light chain. The resulting Scarlett mouse strain
315 displayed circulating human IgG1 concentrations comparable to those of mouse IgG1 in
316 C57BL/6J mice. We note however that even though the Scarlett model produce levels of
317 human IgG1 comparable to what is physiologically relevant for mouse IgG1, it may
318 nonetheless somewhat underestimate the impact of competing IgG1 in humans due to species
319 differences since humans produce higher levels of this antibody isotype. . Beyond their utility
320 in comparing the PK of different half-life extension variants as shown here, these new knock-
321 in models are likely to prove particularly useful for preclinical studies for the understanding
322 of antibody effector functions in mice that express physiologically relevant levels of hFcγRs
323 and additionally express competing endogenous IgG1.

Consistent with the improved PK properties of antibodies with the DHS mutations compared to antibodies with the clinical-stage YTE and LS variants in Tg276 hemizygous mice in **Fig. 1d** and **Table 2**, the DHS amino acid substitutions resulted in ≥ 50% increase β phase $T_{1/2}$ and AUC_{inf} in the Scarlett model. The relative improvement in the PK parameters of DHS antibodies compared to the YTE or LS variants in the Scarlett model was lower than the effect (2-fold) observed in Tg276 and may be due to competition by IgG, the impact of effector FcγR clearance mechanisms and possibly, mouse strain background differences. If, as expected, the pharmacokinetic behavior of antibodies in Scarlett mice more closely mimics that in humans, the observed 50% greater β-phase half-life and drug exposure afforded by the DHS mutations should result in significant therapeutic benefit. For example, a 50% improvement over YTE antibodies[28] could be expected to translate into a circulation half-life in humans of well over 100 days.

To quantitatively explore the significance of endosomal retention (determined by K_D at pH 5.8) versus surface recapture (determined by the K_D at pH 7.4) we constructed a simple phenomenological PK model (**Supplementary Fig. 10**). This model is sufficient to explain the relative PK properties of each Fc domain. Sensitivity analysis indicates that surface recapture is the dominant parameter limiting circulation persistence of YTE- and LS-IgG1 mutants. Specifically, in the hemizygotic Tg276 mice as well as in the Scarlett mice, the consequence of residual affinity of these Fc domains at the extracellular pH is roughly 50% or 20% recapture, respectively, of antibody on the cell surface during endosomal recycling. Collectively, both experimental PK comparison and the quantitative modeling of antibodies with distinct hFcRn binding properties at endosomal and physiological pH highlight the negative effect of hFc:hFcRn binding at pH 7.4 on antibody circulation persistence.

Fc-mediated effector functions (ADCC and CDC), developability (biophysical properties including thermodynamic stability), and drug bioavailability (serum half-life/AUC_{inf}) are of critical importance for clinical application of therapeutic antibodies[58,64]. We demonstrate herein that the DHS Fc variant has (i) intact Fc-mediated effector functions, (ii) a similar Tm, low aggregation propensity, no evidence for self-association and low binding to rheumatoid factor, similar to wt IgG1 antibodies, and (iii) ultra-long circulation persistence in highly relevant new humanized mouse models.

MATERIALS AND METHODS

Cells and Reagents

Adenocarcinoma SK-BR3 cell line (ATCC® HTB-30™) and Raji cell line (ATCC® CCL-86™) were obtained from American Type Culture Collection. SK-BR3 was cultured in complete DMEM with 10 % fetal bovine serum (FBS) and Raji was cultured in complete RPMI 1640 with 10 % FBS. Human PBMCs were purified from anonymous healthy volunteers using Histopaque density gradient centrifugation (Sigma-Aldrich). Human C1q (CompTech) and hFcRn:hβ2m (Novus Biologicals) were purchased. All primers were synthesized by Integrated DNA Technologies.

Preparation of recombinant proteins

Human Fc receptors including hFcγRI, hFcγRIIa, hFcγRIIb, hFcγRIIIa, and hFcRn:hβ2m were cloned in-frame into the mammalian expression vector pcDNA3.4 using Gibson Assembly cloning (NEB)[44] and were produced by transient transfection of Expi293 cells (Invitrogen) according to the manufacturer's instruction[43,4465]. His-tagged Fc receptor proteins were purified with Ni-NTA (GE Healthcare) affinity columns and GST-tagged Fc receptor proteins were purified with Glutathione Sepharose (GE Healthcare) affinity columns according to the manufacturer's instructions. In order to remove lipopolysaccharide (LPS) and non-specifically bound protein, the Fc receptor-bound resins were washed with 50 mL of PBS containing 0.1% Triton®X-114 (Sigma-Aldrich) and 50 mL of PBS. His-tagged Fc receptor proteins were eluted with PBS containing 250 mM imidazole and GST-tagged Fc receptor proteins were eluted with PBS containing 10 mM reduced L-glutathione. The buffer in the Fc receptor protein containing eluent fraction was exchanged with PBS by Amicon Ultra-30 centrifugal spin columns (Milipore).

Similarly, isolated Fc candidates were cloned in-frame into the mammalian expression vector pcDNA3.4-IgH-Trastuzumumab using Gibson Assembly cloning (NEB)[66] and were produced in Expi293 cells (Invitrogen) grown for 5 days at 37°C with 8 % CO_2. All IgG variants proteins purified by Protein A high capacity agarose resin (Thermo Scientific) according to the manufacturer's instructions. Purity of antibody variants was confirmed by SDS-PAGE and size exclusion chromatography and was over 95 %.

Library Construction and screening

Amino acid residues D249-R255, V308-L314, E430-Q438 in the Fc that are within 7Å distance from FcRn in the crystal structure of the human Fc:FcRn complex (PDB ID: 4N0U)[13] were selected for mutagenesis using the aa substitution scheme shown and three separate libraries were constructed using primers with degenerate codons (**Supplementary Table 1**). The heavy chain of trastuzumab IgG1 was used as the template. The amplified PCR fragments were ligated into pPelB-AglycoT(H)-FLAG[43] with *Sfi*I restriction sites for the histidine scanning library. The resulting plasmids were transformed into *E. coli* Jude-1(F' [Tn*10(*Tet^r*)* proAB$^+$ *lacI*^{q} Δ(*lacZ*)M15] *mcrA* Δ(*mrr-hsdRMS-mcrBC*) 80d*lacZ*ΔM15 Δ*lacX74 deoR recA1 araD139* Δ(*ara leu*)7697 *galU galK rpsL endA1 nupG*) harboring pBAD-AglycoT(L)-His[43,67] to display both heavy and light chain of aglycosylated IgG1 in periplasm anchored on the inner membrane via the NlpA signal peptide (APEx display)[45]. Following electroporation 1×10^8 transformants were obtained. The transformants were spheroplasted after overnight induction with 1mM of IPTG and 0.2% of L-arabinose, followed by screening with 10 nM of hFcRn:hβ2m, conjugated with fluorescent Alexa488 (hFcRn:hβ2m Alexa488) as a target probe, at pH 5.8 in PBS. Screening was performed using a FACSAria™ (BD Biosciences). In each round, the top 3 % of the population showing the highest fluorescence was collected and the spheroplasts were re-sorted immediately to

remove false positives. The transformants with the plasmids of sorted spheroplasts were prepared. After 4 rounds, in order to achieve pH-selective binding activity, the library was first labeled with 5 nM of GST- hFcRn:hβ2m-Alexa647 at neutral pH, then incubated with 10 nM of hFcRn:hβ2m -Alexa488 at pH 5.8 (**Fig. 1a**). After the 5th round, single Fc variants were analyzed with pH-dependent binding activities by flow cytometry and the four candidates were isolated.

LC-ESI-MS/MS analysis of Fc variants

Fc proteins were analyzed by The University of Texas at Austin Proteomics Facility using LC-MS on Thermo Orbitrap Fusion Tribrid mass spectrometer with the FT detector. A fast gradient of 0.1% formic acid/water and 0.1% formic acid/acetonitrile over 10 minutes was used to elute the intact proteins from an OPTI-TRAP^{TM} protein microtrap (Optimize Technologies). The Orbitrap Fusion was operated in Intact Protein Mode at 15,000 resolution from 400-2000 m/z. The data was deconvoluted using Thermo Protein Deconvolution software.

Size exclusion chromatography

SEC analyses for the purified IgG proteins were performed on an ÄKTA Pure (GE Healthcare) liquid chromatography system using a Superdex 200 10/300GC, (GE Healthcare), with a mobile phase of pH 7.4 PBS at a flow rate of 0.75 mL/min. Chromatograms were obtained by monitoring the absorbance at 280 nm. The injection amount was 100 μg of proteins in a volume of 200 μL. For thermal stress test, each antibody protein (1 mg/ml) was incubated at 70°C for 10, 20, 40 and 60 min and then analyzed by SEC using the above described method.

Differential scanning fluorimetry (DSF)

DSF was performed with SYPRO Orange dye (Catalog #S-6650, Life Technologies) to determine the thermal stability by monitoring the protein unfolding of the purified Fc domains. For each sample, 15 μL of Fc domains varying from 0.08 to 20 μM were mixed with 5 μL of dye, diluted from 5000× to 20× for use. Each experiment included a control without proteins containing 100 mM HEPES buffer at pH 7. The DSF assays were performed on an Applied Biosystems ViiA 7 Real-Time PCR System using a temperature gradient from 25°C to 99°C at a temperature ramp rate of 0.03°C/s. The fluorescence emissions and melting temperature measurements were analyzed using ViiA 7 Software from Life Technologies.

AC-SINS

Goat anti-human Fc fragment specific (Jackson ImmunoResearch, 109-005-008) was buffer exchanged into 20 mM potassium acetate (pH 4.3) twice using Zeba desalting columns (Thermo Fisher Scientific, PI-89882). The goat anti-human Fc concentration was evaluated using UV absorbance value at 280 nm (extinction coefficient of 1.26 mL/mg*cm). The polyclonal antibody was diluted to 0.4 mg/mL in the acetate buffer. Equal volumes of goat anti-human Fc antibody and gold nanoparticles (Ted Pella, 15705-1) were incubated at room temperature (1 h). The antibody-gold conjugates (3 mL) were loaded onto 0.22 μm filters (Millipore Sigma, SLGV013SL, PVDF), resulting in the retention of the conjugates on the filter membrane. PBS buffer (150 μL) was added to the filter cartridges to elute the gold conjugates, which typically resulted in recovery of ~100 μL per cartridge. The concentrated conjugates were mixed well by pipetting up and down ten times. The conjugates (5 μL) were added first to a 384-well polystyrene plate (Thermo Fisher, 12-565-506), and then the PBS control or test antibodies (in PBS, 45 μL) were added. The samples were mixed well by pipetting up and down ten times. The absorbance spectra were measured (450-650 nm) in 1 nm increments using a Biotek Synergy Neo microplate reader (BioTek, Winooski VT). The

plasmon wavelengths were calculated by fitting a second order polynomial equations to the 40 absorbance measurements surrounding the maximum absorbance values and setting the first derivatives of the polynomials to zero. The plasmon shifts were calculated as the difference in the plasmon wavelengths of the test antibodies relative to the PBS control (no human antibody).

hFc:hFcRn KD determination using surface plasmon resonance (SPR)

For SPR analysis, IgG1 antibody variants were immobilized on CM5 chip surface at a density of ~500 response units (RU) via an amine coupling. hFcRn:hβ2m dimer (Novus Biologicals) was injected at serially diluted concentrations (1000 nM – 40 nM) in PBS, pH 5.8, at a flow rate of 30 μL/min. To examine the interaction of hFcRn and antibody variants at physiological pH 7.4, hFcRn:hβ2m dimer (Novus Biologicals) was immobilized on the BIACore Chip at three different densities, 500 RU, 2000 RU, and 4000 RU via amine coupling[11]. Serially diluted antibodies (800 – 50 nM) were injected in PBS, pH 7.4, at a flow rate of 30 μL/min. Dissociation constants (K_Ds) were determined by fitting the corresponding binding isotherms for steady-state data or by fitting the kinetics for association and dissociation employing a 1:1 Langmuir mass transfer model. In addition, to detect the function of pH for hFc:hFcRn interaction, 800 nM of each antibody variants was injected under diverse pH conditions (pH 6.0-8.0) and RU_{max} was measured.

ELISA assays

50 μl of 2 μg/ml antibody variant was diluted in PBS (pH 7.4) and used to coat 96 well polystyrene ELISA plate (Corning, Corning, NY) overnight at 4°C. After blocking with PBS (pH 7.4) with 3 % bovine serum albumin (BSA) for 1 hour at room temperature, the plate was washed 4 times with PBS containing 0.05% Tween20 (PBST) and incubated with

serially diluted GST- hFcRn:hβ2m, His-tagged hFcγRI, GST-tagged hFcγRIIa, GST-tagged hFcγRIIb, or GST-tagged hFcγRIIIa in PBS (pH 7.4) at room temperature for 1 hour. After washing 4 times with PBST, either 1:10,000 diluted HRP conjugated anti-His or anti-GST antibody (Rockland Immunochemicals) was added, and plates were washed with PBST. Absorbance at 450 nm was measured after development with TMB substrate (Pierce Biotechnology, Rockford, IL) according to the manufacturer's instructions.

Rheumatoid factor (RF) binding assays

50 µl of RF positive serum (Lee Biosolutions), obtained from three different RA patients, was coated in 96 well polystyrene ELISA plate (Corning, NY) overnight at 4°C. After a blocking and washing step, plates were incubated with biotinylated antibody variants for 1 hour at room temperature. The binding was detected by streptavidin-HRP and TMB substrate (Thermo Fisher Scientific) according to the manufacturer's instructions.

ADCC assays

Her2-overexpressing SK-BR3 breast cancer cells were cultured in complete DMEM and collected by centrifugation at 300× g for 5 min. The harvested SK-BR-3 cells were washed in PBS and labeled with 4 µM Calcein AM (Life Technologies, USA) in PBS at 37°C under 5% CO_2 for 30 min. The Calcein loaded SK-BR-3 cells were washed twice, resuspended in RPMI medium, and seeded into a 96-well plate at 10,000 cells/well. The various concentrations of IgG variants were also added. PBMCs were isolated from human blood from healthy donors. Briefly, 50 mL of human blood was collected in heparinized vials (BD biosciences) and mixed by gently inverting the tube several times. 25 mL of blood was layered over 25 mL of Histopaque (Sigma-Aldrich) in 50 mL conical tubes. The tubes were centrifuged at 400 g for 10 min in a swing-out bucket with no brakes. The human PBMCs were aspirated in the

interphase between histopaque and medium. Human PBMCs were resuspended with red blood cell (RBC) lysis buffer (155 mM NH_4Cl, 12 mM $NaHCO_3$, and 0.1 mM EDTA), and washed twice with PBS. PBMCs were transferred into a 96-well plate at 100,000 cells/well (the ratio of tumor versus PBMCs was 1:10), and the plates were incubated at 37°C under 5% CO_2 for 4 hours. The released calcein AM was detected at excitation and emission wavelengths of 485 nm and 535 nm. The percent of tumor cell lysis was calculated according to the following formula; (1) $100 \times (E-S) \times (M-S)^{-1}$, where E is the fluorescence of experimental well, S is the fluorescence of a well containing tumor cells and complement but no antibody, and M is the fluorescence of a well containing tumor cells with lysis buffer (Triton X-100 at 2% v/v, SDS 1% w/v, 100mM NaCl, and 1mM EDTA). As an isotype control, Rituximab was used.

C1q deposition assay

Raji cells were resuspended in 25% human serum and then incubated with the serially diluted Rituximab-Fc variants at 37 °C for 30 min. Classical complement activation reactions were then quenched with 20 volumes of ice-cold 1% BSA-PBS. The cells were pelleted, washed once, and then probed with FITC anti-C1q (Abcam) for 30 min at 4 °C. The samples were washed and analyzed by flow cytometry.

CDC assay

For CDC assay, Raji cells were labeled with 4 μM Calcein AM (Life Technologies, USA) in PBS at 37°C under 5% CO_2 for 30 min and serially diluted Rituximab variants were incubated with 25% human serum and calcein AM-loaded Raji cells at 37°C for 1 h in 96-well plates. The supernatants were collected after centrifugation at 1,000*g* for 10 min. The

fraction of lysed Raji cells was determined by the same method as used for the ADCC assays. As an isotype control, Trastuzumab was used.

Mice

Hemizygous hFcRn transgenic mice (line 276; aka Tg276) were generated by the F1 cross of murine FcRn deficient B6.129X1-*Fcgrttm1Dcr*/DcrJ and hFcRn transgenic line (generated by random integration of the hFcRn cDNA) B6.Cg-*Fcgrttm1Dcr* Tg (CAG-*FCGRT*) 276 Dcr/DcrJ (The Jackson laboratory)[5,68]. Tg276 mice experiments were performed under a protocol approved by UT Austin institutional Animal Care and Use Committee (IACUC). hFcγR^{KI} mice[51] were generated by Regeneron Pharmaceuticals Inc. to express hFcγRI, hFcγRIIa$_{H131}$, hFcγRIIb$_{I232}$, hFcγRIIc$_{stop13}$, hFcγRIIIa$_{V158}$ and hFcγRIIIb$_{NA2}$ polymorphic variants, as described previously[51]. hFcRn^{KI} (VG1481) and hβ2m^{KI} (VG5153) were designed and generated by Regeneron Pharmaceuticals Inc. on a mixed 62.5% C57BL/6N and 37.5% 129S6/SvEv genetic background. hIgG1-heavy chain^{KI} (hIgG1^{KI}) were generated on a BALB/c background in the Cogné lab. Human kappa-light chain^{KI} (*Igκ*^{KI}) were generated on a C57BL/6N background in the Bruhns lab. Mice were intercrossed at Institut Pasteur (Bruhns lab) to generate Marlene (hFcRn^{KI} hβ2m^{KI} hFcγR^{KI}) or Scarlett (hFcRn^{KI} hβ2m^{KI} hFcγR^{KI} hIgG1,κ^{KI}) mice and used for experiments at 10 to 18 weeks of age. FcγR^{null} mice expressing no FcγRs were used as controls. All mouse models demonstrated normal development and breeding patterns and hFcγR expression on different cell populations from the spleen were confirmed, as described previously[51].

Experiments using knock in mice were validated by the Comité d'Éthique en Expérimentation Animale (CETEA) #89 (Institut Pasteur, Paris, France) under #2013-0103 and by the French Ministry of Research under agreement #00513.02.

Endogenous mouse or human IgG detection in knock-in mice

Goat anti-human IgG-Fc fragment antibodies (1 μg) or goat anti-mouse IgG-Fc fragment antibodies (0.2 μg) were diluted in carbonate buffer (pH 9.6) (Bethyl Laboratories, Montgomery, TX) and used to coat MaxiSorp 96 well ELISA plates (Nunc, ThermoFischer scientific, Waltham, MA) overnight at 4°C. After blocking with PBS with 3% BSA for 1 hour at room temperature, plates were washed 3 times with PBST and incubated with serially diluted wt or KI mouse serum (or human and mouse reference serum as quantification standards), at room temperature for 3 hours. After washing, HRP-conjugated anti-human IgG (diluted 1:20,000, Bethyl Laboratories Inc.) or anti-mouse IgG (diluted 1:10,000, Bethyl Laboratories Inc.) were added, and plates were washed with PBST. Absorbance at 492 vs 620 nm was measured after development with the OPD substrate (Sigma Aldrich, Saint-Louis, MO).

Immunohistochemistry

Spleens were fixed in 10% neutral buffered formalin for 24h and embedded in paraffin. Tissue sections (4μm) were blocked in PBS containing 3% BSA. Sections were stained with either an anti-human FcRn antibody (4μg/mL, Novus Biologicals) or an anti-mouse FcRn antibody (100×, R&D Systems) for 30 min at 37°C. Primary antibodies were detected with appropriate peroxidase-conjugated secondary antibodies and DAB detection kit (<8min, RT). All staining reactions were accompanied by a negative control that consisted of an isotype-matched irrelevant antibody. Stained slides were evaluated with a light microscope (Nikon).

RT PCR

Total RNA was extracted from human peripheral blood mononuclear cells or murine splenocytes using NucleoSpin RNA plus kit (Macherey-Nagel) according to the

563 manufacturer's recommendations. cDNAs were generated at 50 °C for 60 minutes using
564 random primers and SuperScript III Reverse Transcriptase (Invitrogen). The primer pairs for
565 the human FcRn gene *FCGRT* (L28-L179) and the mouse FcRn gene *Fcgrt* (L231-R295)
566 (*FCGRT*: 5'-CTCTCCCTCCTGTACCACCTT-3'; 5'-ATAGCAGGAAGGTGAGCTCCT-3';
567 *Fcgrt*: 5'-AGCTCAAGTTCCGATTCCTG-3'; 5'- GATCTGGCTGATGAATCTAGGTC-3')
568 were used for amplification with GoTaq G2 polymerase (Promega). Amplification was
569 performed by 35 cycles PCR each consisting of 94 °C for 1 min, 58 °C for 1 min, 72 °C for 1
570 min. At the end of the 35 cycles, samples were run for an additional 10 min at 72 °C and
571 analyzed by 1.5 % agarose gel electrophoresis.

572 **Pharmacokinetics studies in mice**

573 Animals were administered a bolus intravenous (i.v.) dose of 2 mg/kg antibody on day 0 by
574 tail vein injection. Blood samples were obtained from the tail vein using capillary pipettes at
575 different time points.

576 Serum concentration of antibody in Tg276, Marlene, or Scarlett was determined using a
577 quantitative ELISA as follows: 96-well plates were coated with 2 μg of Goat anti-human
578 $F(ab')_2$ fragment-specific $F(ab')_2$ (for Tg276, Jackson Immunoresearch) or 1 μg of each
579 antigens (for Marlene and Scarlett). Her2 extracellular domain protein (Antibodies-Online)
580 for trastuzumab, CD20 linear peptide (142-184, extracellular domain, Alpha Diagnostic Intl.,
581 Inc.) for rituximab, or IgE protein for omalizumab was used. Plates were blocked with 1%
582 Fish gelatin (AMRESCO Inc) in PBS for 1 hour, and then incubated with appropriately
583 diluted serum samples (1:200 for earlier time points and 1:50 or 1:100 for later time points).
584 Anti-kappa light chain antibody-HRP (Abcam) was used to detect the human antibody
585 (dilution 1:5,000). Absorbance at 450 nm was measured after development with TMB
586 substrate (Pierce Biotechnology, Rockford, IL) according to manufacturer's directions.

Standard curves were generated for each antibody variant diluted into 1:100 pre-bleed mouse serum. The linear portions of standard curves generated in Prism (GraphPad Software) were then used to quantify human IgG in the serum samples.

Pharmacokinetic parameters were analyzed with a two-compartment elimination model. AUC_{inf} (area under the curve to infinity) was calculated using the log-linear trapezoidal method[20]. Terminal half-life ($T_{1/2}$) was calculated using two-phase clearance models. Log-linear regression of the concentration data including at least the last six sampling time-points with measurable concentrations. Serum clearance was estimated as: (2) $CL=DoseAUC_{inf}^{-1}$. Volumes of distribution at steady state were calculated using the following equation: (3) $Vss=Dose \times AUMC_{inf} \times (AUC_{inf})^{-2}$.

Computational Modeling

All analysis was implemented in R and Stan, and can be found at [https://github.com/meyer-lab/FcRn-trafficking], release 1.0 (doi: 10.5281/zenodo.3474026). Test conditions were identified throughout to ensure model accuracy.

Exogenous IgG trafficking was modeled according to the following relationships, consistent with the graphic presented in **Supplementary Fig. 10**. Exogenous IgG is modeled to exchange between three compartments representing a central extracellular, peripheral extracellular, and endosomal space. The central compartment is modeled as:

$$(4)\ \frac{\delta C_c}{\delta t} = Q(C_p - C_c)$$

where C_c, C_p, and C_e indicate the central, peripheral, and endosomal compartment concentrations, respectively, in units of μg/mL. Q indicates the transport rate between these two compartments in units of the central compartment volume per hour. As the entire model scales proportionally, the central compartment volume (V_c) was assumed to equal 1, and all

volumes are specified in relative amounts. The peripheral compartment concentration was specified as:

$$(5)\ \frac{\delta C_p}{\delta t} V_p = QC_c - QC_p - Q_u C_p + Q_u C_e f_{sort} f_{release}$$

where V_p and V_e are the peripheral and endosomal volumes (relative to the central compartment volume), and Q_u is the rate of uptake into cells in units of central compartment volume per hour.

f_{sort} indicates the fraction of endosomal IgG that is recycled, and $f_{release}$ indicates the fraction of IgG presented to the cell surface that is released (as opposed to endocytosed again).

$$(6)\ \frac{\delta C_e}{\delta t} V_e = Q_u \left[C_p + C_e[(1 - f_{release}) f_{sort} - 1] \right]$$

Implicit in this model are a few assumptions: First, there is no clearance outside of cellular uptake and lysosomal degradation. Each sorting fraction and model parameter is assumed to not vary with the concentration of exogenous IgG, therefore assuming that the modeled processes are not saturable. Finally, sorting and release are assumed to vary in the same order as their measured affinities at pH 5.8 and 7.4, with IgG of no measurable affinity at 7.4 fully released ($f_{release} = 1$).

The resultant linear ODE model was solved using the matrix exponential of the Jacobian. The half-life was found through root finding with Newton's method. Model fitting was performed using Markov Chain Monte Carlo within Stan[69]. Priors on V_p, Q, and $V_i n$ were all specified as log-normal distributions with a mean and deviation of 1 in their respective units. The prior for Q_u was specified as a log-normal distribution with mean $e^{0.1}$ and deviation of 0.5. Sorting parameter priors were specified to be flat and constrained to be in the order dictated by their relative affinity measurements.

For example, if species A had a higher endosomal affinity than B, then $f_{sort,A}$ was given an even prior from 0 to 1, and $f_{sort,B}$ was given an even prior from 0 to $f_{sort,A}$. The half-life of each species was compared to a normal distribution representing the average and standard error of the *in vivo* experimental measurements. Sampling convergence was verified through autocorrelation analysis and the Geweke criterion.

Acknowledgements

We thank Y. Tanno for assistance with protein expression and M. Tichit with immunohistochemistry assay. This work was supported by the Clayton Foundation, by the European Research Council (ERC)–Seventh Framework Program (ERC-2013-CoG 616050 to P.B.), by the Institut Pasteur and the Institut National de la Santé et de la Recherche Médicale (INSERM). P.M.T was supported by the National Institutes of Health (R01GM104130), National Science Foundation (CBET 1804313) and the Albert M. Mattocks Chair. A.M. was supported by NIH DP5-OD019815. C.M.G was supported partly by a stipend from the Pasteur–Paris University (PPU) International PhD program and by the Institut Carnot Pasteur Maladies Infectieuses. D.S. benefited from a stipend (Poste d'accueil) provided by AP-HP, Paris, France and by the Institut Pasteur, Paris, France.

Author Contributions

G.G., P.B., C.-H.L., and T.H.K. conceived and designed the research; C.-H.L., T.H.K., O.G., M.W., G.D., C.M.G., D.S., D.H., A.J.M., N.T., J.L. and E.M. performed experiments; G.G., P.B., C.-H.L., O.G., M.W., G.D., C.M.G., D.S., M.C., L.E.M., A.J.M., J.R.M., P.M.T., and A.S.M. analyzed data. G.G., P.B., C.-H.L., M.W., and G.D. wrote the paper. G.G. and P.B. provided funding.

Competing Financial Interests

G.G., C.-H.L., and T.H.K. declare competing financial interests (PCT/US2019/0048078). The other authors declare no competing interests.

Data availability

All the other data that support the findings of this study are available from the corresponding author upon request.

Code availability

All analysis for computational modeling was implemented in R v3.5.3 and rstan v2.18.2, and can be found at [https://github.com/meyer-lab/FcRn-trafficking], release 1.1 (doi: 10.5281/zenodo.3474026). The code is available for access under the MIT license without restrictions.

669 **References**

670

671 1. Ghetie, V. & Ward, E. S. Multiple Roles for the Major Histocompatibility Complex Class I– Related
672 Receptor FcRn. *Annu. Rev. Immunol.* **18**, 739–766 (2000).
673 2. Roopenian, D. C. & Akilesh, S. FcRn: the neonatal Fc receptor comes of age. *Nat. Rev. Immunol.* **7**,
674 715–725 (2007).
675 3. Ward, E. S., Devanaboyina, S. C. & Ober, R. J. Targeting FcRn for the modulation of antibody
676 dynamics. *Mol. Immunol.* **67**, 131–141 (2015).
677 4. Pyzik, M., Rath, T., Lencer, W. I., Baker, K. & Blumberg, R. S. FcRn: The Architect Behind the
678 Immune and Nonimmune Functions of IgG and Albumin. *J. Immunol. Baltim. Md 1950* **194**,
679 4595–4603 (2015).
680 5. Roopenian, D. C. *et al.* The MHC Class I-Like IgG Receptor Controls Perinatal IgG Transport, IgG
681 Homeostasis, and Fate of IgG-Fc-Coupled Drugs. *J. Immunol.* **170**, 3528–3533 (2003).
682 6. D'Hooghe, L., Chalmers, A. D., Heywood, S. & Whitley, P. Cell surface dynamics and cellular
683 distribution of endogenous FcRn. *PloS One* **12**, e0182695 (2017).
684 7. Challa, D. K., Velmurugan, R., Ober, R. J. & Sally Ward, E. FcRn: from molecular interactions to
685 regulation of IgG pharmacokinetics and functions. *Curr. Top. Microbiol. Immunol.* **382**, 249–272
686 (2014).
687 8. Lencer, W. I. & Blumberg, R. S. A passionate kiss, then run: exocytosis and recycling of IgG by
688 FcRn. *Trends Cell Biol.* **15**, 5–9 (2005).
689 9. Sánchez, L. M., Penny, D. M. & Bjorkman, P. J. Stoichiometry of the interaction between the
690 major histocompatibility complex-related Fc receptor and its Fc ligand. *Biochemistry* **38**, 9471–
691 9476 (1999).
692 10. Abdiche, Y. N. *et al.* The neonatal Fc receptor (FcRn) binds independently to both sites of the IgG
693 homodimer with identical affinity. *mAbs* **7**, 331–343 (2015).

694 11. Walters, B. T. *et al.* Conformational Destabilization of Immunoglobulin G Increases the Low pH
695 Binding Affinity with the Neonatal Fc Receptor. *J. Biol. Chem.* **291**, 1817–1825 (2016).
696 12. Martin, W. L., West Jr., A. P., Gan, L. & Bjorkman, P. J. Crystal Structure at 2.8 Å of an
697 FcRn/Heterodimeric Fc Complex: Mechanism of pH-Dependent Binding. *Mol. Cell* **7**, 867–877
698 (2001).
699 13. Oganesyan, V. *et al.* Structural Insights into Neonatal Fc Receptor-based Recycling Mechanisms.
700 *J. Biol. Chem.* **289**, 7812–7824 (2014).
701 14. Morgan, P. *et al.* Can the flow of medicines be improved? Fundamental pharmacokinetic and
702 pharmacological principles toward improving Phase II survival. *Drug Discov. Today* **17**, 419–424
703 (2012).
704 15. Kamath, A. V. Translational pharmacokinetics and pharmacodynamics of monoclonal antibodies.
705 *Drug Discov. Today Technol.* **21–22**, 75–83 (2016).
706 16. Zalevsky, J. *et al.* Enhanced antibody half-life improves in vivo activity. *Nat. Biotechnol.* **28**, 157–
707 159 (2010).
708 17. Dall'Acqua, W. F. *et al.* Increasing the affinity of a human IgG1 for the neonatal Fc receptor:
709 biological consequences. *J. Immunol. Baltim. Md 1950* **169**, 5171–5180 (2002).
710 18. Dall'Acqua, W. F., Kiener, P. A. & Wu, H. Properties of Human IgG1s Engineered for Enhanced
711 Binding to the Neonatal Fc Receptor (FcRn). *J. Biol. Chem.* **281**, 23514–23524 (2006).
712 19. Strohl, W. R. Current progress in innovative engineered antibodies. *Protein Cell* **9**, 86–120 (2018).
713 20. Borrok, M. J. *et al.* pH-Dependent Binding Engineering Reveals An FcRn Affinity Threshold Which
714 Governs IgG Recycling. *J. Biol. Chem.* jbc.M114.603712 (2014) doi:10.1074/jbc.M114.603712.
715 21. Ghetie, V. *et al.* Increasing the serum persistence of an IgG fragment by random mutagenesis.
716 *Nat. Biotechnol.* **15**, 637–640 (1997).

22. Robbie, G. J. *et al.* A Novel Investigational Fc-Modified Humanized Monoclonal Antibody, Motavizumab-YTE, Has an Extended Half-Life in Healthy Adults. *Antimicrob. Agents Chemother.* **57**, 6147–6153 (2013).
23. Datta-Mannan, A. *et al.* FcRn Affinity-Pharmacokinetic Relationship of Five Human IgG4 Antibodies Engineered for Improved In Vitro FcRn Binding Properties in Cynomolgus Monkeys. *Drug Metab. Dispos.* **40**, 1545–1555 (2012).
24. Zhu, Q. *et al.* A highly potent extended half-life antibody as a potential RSV vaccine surrogate for all infants. *Sci. Transl. Med.* **9**, (2017).
25. Ko, S.-Y. *et al.* Enhanced neonatal Fc receptor function improves protection against primate SHIV infection. *Nature* **514**, 642–645 (2014).
26. Vaccaro, C., Bawdon, R., Wanjie, S., Ober, R. J. & Ward, E. S. Divergent activities of an engineered antibody in murine and human systems have implications for therapeutic antibodies. *Proc. Natl. Acad. Sci.* **103**, 18709–18714 (2006).
27. FDA approved | PNH treatment. https://www.ultomiris.com/?gclid=EAIaIQobChMItYL2pNyK5QIVUL7ACh0R3ANREAAYASAAEgJANPD_BwE.
28. Domachowske, J. B. *et al.* Safety, Tolerability, and Pharmacokinetics of MEDI8897, an Extended Half-Life Single-Dose Respiratory Syncytial Virus Prefusion F-Targeting Monoclonal Antibody Administered as a Single Dose to Healthy Preterm Infants. *Pediatr. Infect. Dis. J.* (2018) doi:10.1097/INF.0000000000001916.
29. Datta-Mannan, A., Witcher, D. R., Tang, Y., Watkins, J. & Wroblewski, V. J. Monoclonal Antibody Clearance IMPACT OF MODULATING THE INTERACTION OF IgG WITH THE NEONATAL Fc RECEPTOR. *J. Biol. Chem.* **282**, 1709–1717 (2007).

30. Datta-Mannan, A. *et al.* Humanized IgG1 Variants with Differential Binding Properties to the Neonatal Fc Receptor: Relationship to Pharmacokinetics in Mice and Primates. *Drug Metab. Dispos.* **35**, 86–94 (2007).
31. Zheng, Y. *et al.* Translational pharmacokinetics and pharmacodynamics of an FcRn-variant anti-CD4 monoclonal antibody from preclinical model to phase I study. *Clin. Pharmacol. Ther.* **89**, 283–290 (2011).
32. Cooper, P. R. *et al.* The contribution of cell surface FcRn in monoclonal antibody serum uptake from the intestine in suckling rat pups. *Front. Pharmacol.* **5**, (2014).
33. Wang, W. *et al.* Monoclonal Antibodies with Identical Fc Sequences Can Bind to FcRn Differentially with Pharmacokinetic Consequences. *Drug Metab. Dispos.* **39**, 1469–1477 (2011).
34. Borrok, M. J. *et al.* An 'Fc-Silenced' IgG1 Format With Extended Half-Life Designed for Improved Stability. *J. Pharm. Sci.* **106**, 1008–1017 (2017).
35. Grevys, A. *et al.* Fc Engineering of Human IgG1 for Altered Binding to the Neonatal Fc Receptor Affects Fc Effector Functions. *J. Immunol.* **194**, 5497–5508 (2015).
36. Roopenian, DerryC., Christianson, GregoryJ., Proetzel, G. & Sproule, ThomasJ. Human FcRn Transgenic Mice for Pharmacokinetic Evaluation of Therapeutic Antibodies. in *Mouse Models for Drug Discovery* (eds. Proetzel, G. & Wiles, M. V.) 103–114 (Springer New York, 2016). doi:10.1007/978-1-4939-3661-8_6.
37. Proetzel, G. & Roopenian, D. C. Humanized FcRn mouse models for evaluating pharmacokinetics of human IgG antibodies. *Methods San Diego Calif* **65**, 148–153 (2014).
38. Latvala, S., Jacobsen, B., Otteneder, M. B., Herrmann, A. & Kronenberg, S. Distribution of FcRn Across Species and Tissues. *J. Histochem. Cytochem. Off. J. Histochem. Soc.* **65**, 321–333 (2017).
39. Andersen, J. T., Daba, M. B., Berntzen, G., Michaelsen, T. E. & Sandlie, I. Cross-species Binding Analyses of Mouse and Human Neonatal Fc Receptor Show Dramatic Differences in Immunoglobulin G and Albumin Binding. *J. Biol. Chem.* **285**, 4826–4836 (2010).

40. Tam, S. H., McCarthy, S. G., Brosnan, K., Goldberg, K. M. & Scallon, B. J. Correlations between pharmacokinetics of IgG antibodies in primates vs. FcRn-transgenic mice reveal a rodent model with predictive capabilities. *mAbs* **5**, 397–405 (2013).
41. Kasturirangan, S. *et al.* Targeted Fcγ Receptor (FcγR)-mediated Clearance by a Biparatopic Bispecific Antibody. *J. Biol. Chem.* **292**, 4361–4370 (2017).
42. Khare, P. *et al.* Myelin oligodendrocyte glycoprotein-specific antibodies from multiple sclerosis patients exacerbate disease in a humanized mouse model. *J. Autoimmun.* **86**, 104–115 (2018).
43. Jung, S. T. *et al.* Effective Phagocytosis of Low Her2 Tumor Cell Lines with Engineered, Aglycosylated IgG Displaying High FcγRIIa Affinity and Selectivity. *ACS Chem. Biol.* **8**, 368–375 (2012).
44. Lee, C.-H. *et al.* IgG Fc domains that bind C1q but not effector Fcγ receptors delineate the importance of complement-mediated effector functions. *Nat. Immunol.* **18**, 889–898 (2017).
45. Harvey, B. R. *et al.* Anchored periplasmic expression, a versatile technology for the isolation of high-affinity antibodies from Escherichia coli-expressed libraries. *Proc. Natl. Acad. Sci. U. S. A.* **101**, 9193–9198 (2004).
46. Kang, T. H. *et al.* An Engineered Human Fc variant with Exquisite Selectivity for FcγRIIIaV158 Reveals that Ligation of FcγRIIIa Mediates Potent Antibody Dependent Cellular Phagocytosis with GM-CSF-differentiated Macrophages. *Front. Immunol.* **10**, (2019).
47. Yu, X. *et al.* Engineering hydrophobic protein-carbohydrate interactions to fine-tune monoclonal antibodies. *J. Am. Chem. Soc.* **135**, 9723–9732 (2013).
48. Monnet, C. *et al.* Selection of IgG Variants with Increased FcRn Binding Using Random and Directed Mutagenesis: Impact on Effector Functions. *Front. Immunol.* **6**, (2015).
49. Grevys, A. *et al.* A human endothelial cell-based recycling assay for screening of FcRn targeted molecules. *Nat. Commun.* **9**, 621 (2018).

50. Gillis, C. M. *et al.* Mechanisms of anaphylaxis in human low-affinity IgG receptor locus knock-in mice. *J. Allergy Clin. Immunol.* **139**, 1253-1265.e14 (2017).
51. Beutier, H. *et al.* Platelets expressing IgG receptor FcγRIIA/CD32A determine the severity of experimental anaphylaxis. *Sci. Immunol.* **3**, eaan5997 (2018).
52. Bruhns, P. Properties of mouse and human IgG receptors and their contribution to disease models. *Blood* **119**, 5640–5649 (2012).
53. Zvaifler, N. J. The Immunopathology of Joint Inflammation in Rheumatoid Arthritis11Original work described in this review has been aided by grants (AM 14916 and AM 05140) from the National Institutes of Health. in *Advances in Immunology* (eds. Dixon, F. J. & Kunkel, H. G.) vol. 16 265–336 (Academic Press, 1973).
54. Ingegnoli, F., Castelli, R. & Gualtierotti, R. Rheumatoid factors: clinical applications. *Dis. Markers* **35**, 727–734 (2013).
55. Newkirk, M. M. Rheumatoid factors: host resistance or autoimmunity? *Clin. Immunol. Orlando Fla* **104**, 1–13 (2002).
56. Lee, D. M. *et al.* Mast cells: a cellular link between autoantibodies and inflammatory arthritis. *Science* **297**, 1689–1692 (2002).
57. Jarasch, A. *et al.* Developability Assessment During the Selection of Novel Therapeutic Antibodies. *J. Pharm. Sci.* **104**, 1885–1898 (2015).
58. Jain, T. *et al.* Biophysical properties of the clinical-stage antibody landscape. *Proc. Natl. Acad. Sci. U. S. A.* **114**, 944–949 (2017).
59. Sule, S. V., Dickinson, C. D., Lu, J., Chow, C.-K. & Tessier, P. M. Rapid analysis of antibody self-association in complex mixtures using immunogold conjugates. *Mol. Pharm.* **10**, 1322–1331 (2013).
60. Liu, Y. *et al.* High-throughput screening for developability during early-stage antibody discovery using self-interaction nanoparticle spectroscopy. *mAbs* **6**, 483–492 (2014).

61. Bruhns, P. *et al.* Specificity and affinity of human Fcγ receptors and their polymorphic variants for human IgG subclasses. *Blood* **113**, 3716–3725 (2009).
62. Overdijk, M. B. *et al.* Crosstalk between Human IgG Isotypes and Murine Effector Cells. *J. Immunol.* **189**, 3430–3438 (2012).
63. Stein, C. *et al.* Clinical chemistry of human FcRn transgenic mice. *Mamm. Genome Off. J. Int. Mamm. Genome Soc.* **23**, 259–269 (2012).
64. Almagro, J. C., Daniels-Wells, T. R., Perez-Tapia, S. M. & Penichet, M. L. Progress and Challenges in the Design and Clinical Development of Antibodies for Cancer Therapy. *Front. Immunol.* **8**, (2018).
65. Feng, Y., Gong, R. & Dimitrov, D. S. Design, expression and characterization of a soluble single-chain functional human neonatal Fc receptor. *Protein Expr. Purif.* **79**, 66–71 (2011).
66. Kelton, W. *et al.* IgGA: a 'cross-isotype' engineered human Fc antibody domain that displays both IgG-like and IgA-like effector functions. *Chem. Biol.* **21**, 1603–1609 (2014).
67. Kawarasaki, Y. *et al.* Enhanced crossover SCRATCHY: construction and high-throughput screening of a combinatorial library containing multiple non-homologous crossovers. *Nucleic Acids Res.* **31**, e126 (2003).
68. Chaudhury, C. *et al.* The major histocompatibility complex-related Fc receptor for IgG (FcRn) binds albumin and prolongs its lifespan. *J. Exp. Med.* **197**, 315–322 (2003).
69. Stan: A Probabilistic Programming Language | Carpenter | Journal of Statistical Software. doi:10.18637/jss.v076.i01.

Figures

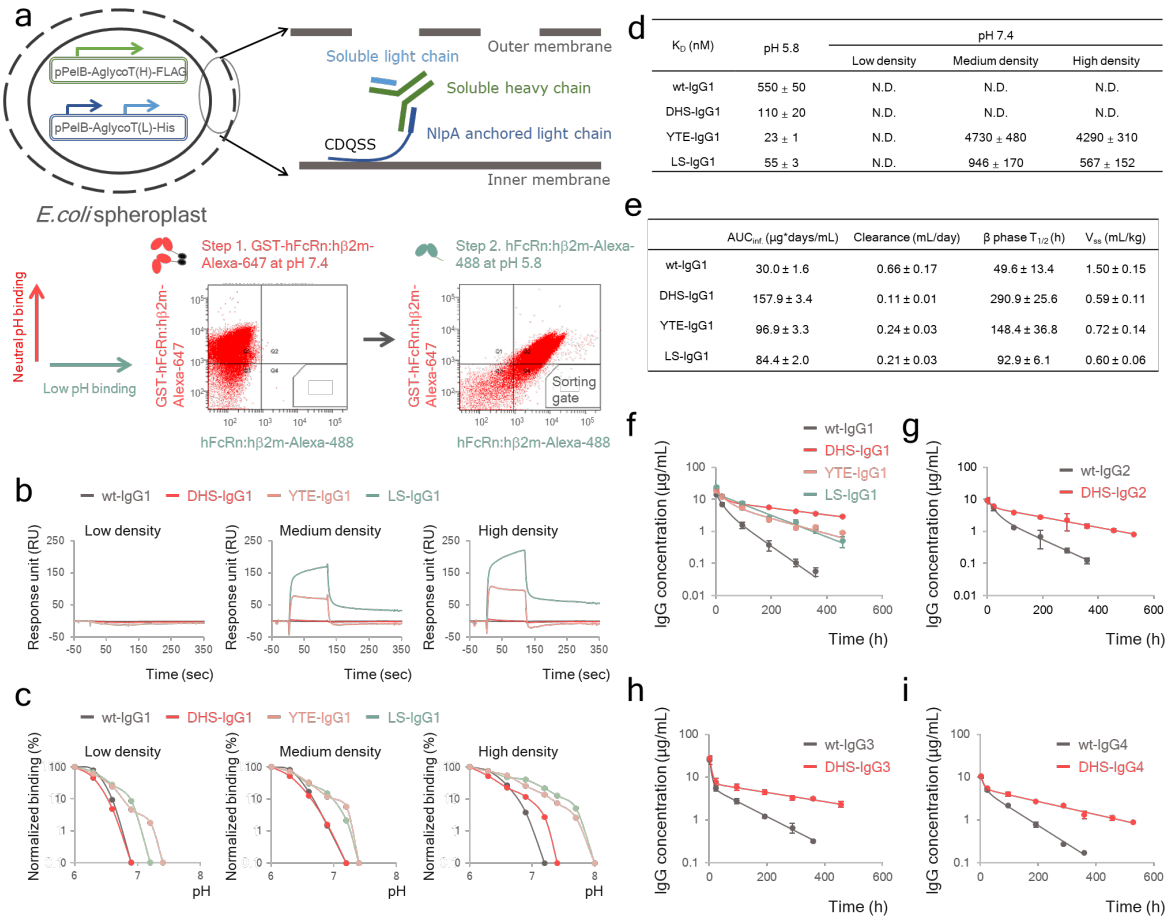

K_D (nM)	pH 5.8	pH 7.4		
		Low density	Medium density	High density
wt-IgG1	550 ± 50	N.D.	N.D.	N.D.
DHS-IgG1	110 ± 20	N.D.	N.D.	N.D.
YTE-IgG1	23 ± 1	N.D.	4730 ± 480	4290 ± 310
LS-IgG1	55 ± 3	N.D.	946 ± 170	567 ± 152

	AUC_{inf} (μg*days/mL)	Clearance (mL/day)	β phase $T_{1/2}$ (h)	V_{ss} (mL/kg)
wt-IgG1	30.0 ± 1.6	0.66 ± 0.17	49.6 ± 13.4	1.50 ± 0.15
DHS-IgG1	157.9 ± 3.4	0.11 ± 0.01	290.9 ± 25.6	0.59 ± 0.11
YTE-IgG1	96.9 ± 3.3	0.24 ± 0.03	148.4 ± 36.8	0.72 ± 0.14
LS-IgG1	84.4 ± 2.0	0.21 ± 0.03	92.9 ± 6.1	0.60 ± 0.06

Figure 1. Engineering a human Fc domain with optimized pH-dependent FcRn binding for ultra-long circulation persistence. (**a**) Screening strategy for the isolation of Fc mutations that confer favorable pH-dependent FcRn-binding using *E.coli* display. (**b-c**) SPR binding of IgG mutants (800 nM) to hFcRn:hβ2m immobilized at low, medium or high density (500, 2000, and 4000 RU, respectively) either, (**b**) at pH 7.4 or (**c**) as a function of pH. Normalized binding intensity was calculated as the pH-dependent RU over the RUmax at pH 6.0, for antibodies at 800nM. Error bars: standard deviation from three independent experiments. (**d-g**) Serum antibody concentration of DHS formatted IgG1 (**d**), IgG2 (**e**), IgG3 (**f**) and IgG4 (**g**) antibodies in hemizygotic Tg276 hFcRn transgenic mice as a function of time after administration. Each antibody variant (2 mg/kg) was administered intravenously to hemizygous Tg276 mice (n=11 for IgG1 and n=5 for IgG2, IgG3 and IgG4). Antibody concentrations were determined by ELISA.. Data are presented as mean ± standard deviation.

851

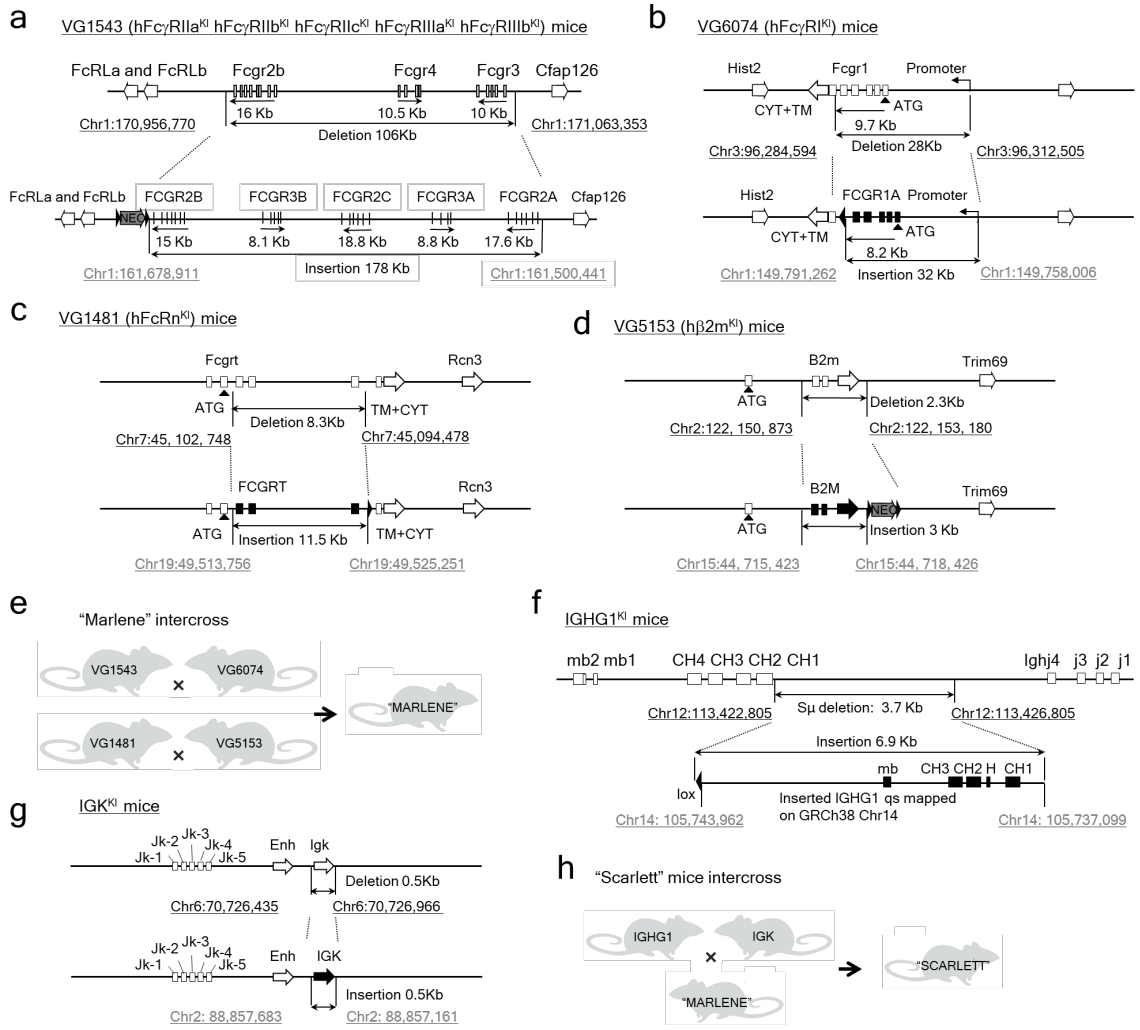
a
VG1543 (hFcγRIIa^KI hFcγRIIb^KI hFcγRIIc^KI hFcγRIIIa^KI hFcγRIIIb^KI) mice
FcRLa and FcRLb
Fcgr2b
Fcgr4
Fcgr3
Cfap126
16 Kb
10.5 Kb
10 Kb
Chr1:170,956,770
Chr1:171,063,353
Deletion 106Kb
FcRLa and FcRLb
FCGR2B
FCGR3B
FCGR2C
FCGR3A
FCGR2A
Cfap126
NEO
15 Kb
8.1 Kb
18.8 Kb
8.8 Kb
17.6 Kb
Chr1:161,678,911
Insertion 178 Kb
Chr1:161,500,441
b
VG6074 (hFcγRI^KI) mice
Hist2
Fcgr1
Promoter
CYT+TM
ATG
9.7 Kb
Chr3:96,284,594
Deletion 28Kb
Chr3:96,312,505
Hist2
FCGR1A
Promoter
CYT+TM
ATG
8.2 Kb
Chr1:149,791,262
Insertion 32 Kb
Chr1:149,758,006
c
VG1481 (hFcRn^KI) mice
Fcgrt
Rcn3
ATG
Deletion 8.3Kb
TM+CYT
Chr7:45, 102, 748
Chr7:45,094,478
FCGRT
Rcn3
ATG
Insertion 11.5 Kb
TM+CYT
Chr19:49,513,756
Chr19:49,525,251
d
VG5153 (hβ2m^KI) mice
B2m
Trim69
ATG
Deletion 2.3Kb
Chr2:122, 150, 873
Chr2:122, 153, 180
B2M
Trim69
NEO
ATG
Insertion 3 Kb
Chr15:44, 715, 423
Chr15:44, 718, 426
e
"Marlene" intercross
VG1543
VG6074
"MARLENE"
VG1481
VG5153
f
IGHG1^KI mice
mb2 mb1
CH4 CH3 CH2 CH1
Ighj4 j3 j2 j1
Chr12:113,422,805
Sμ deletion: 3.7 Kb
Chr12:113,426,805
Insertion 6.9 Kb
mb
CH3 CH2 H CH1
lox
Inserted IGHG1 qs mapped on GRCh38 Chr14
Chr14: 105,743,962
Chr14: 105,737,099
g
IGK^KI mice
Jk-2
Jk-3
Jk-4
Jk-1
Jk-5
Enh
Igk
Deletion 0.5Kb
Chr6:70,726,435
Chr6:70,726,966
Jk-2
Jk-3
Jk-4
Jk-1
Jk-5
Enh
IGK
Insertion 0.5Kb
Chr2: 88,857,683
Chr2: 88,857,161
h
"Scarlett" mice intercross
IGHG1
IGK
"MARLENE"
"SCARLETT"

852

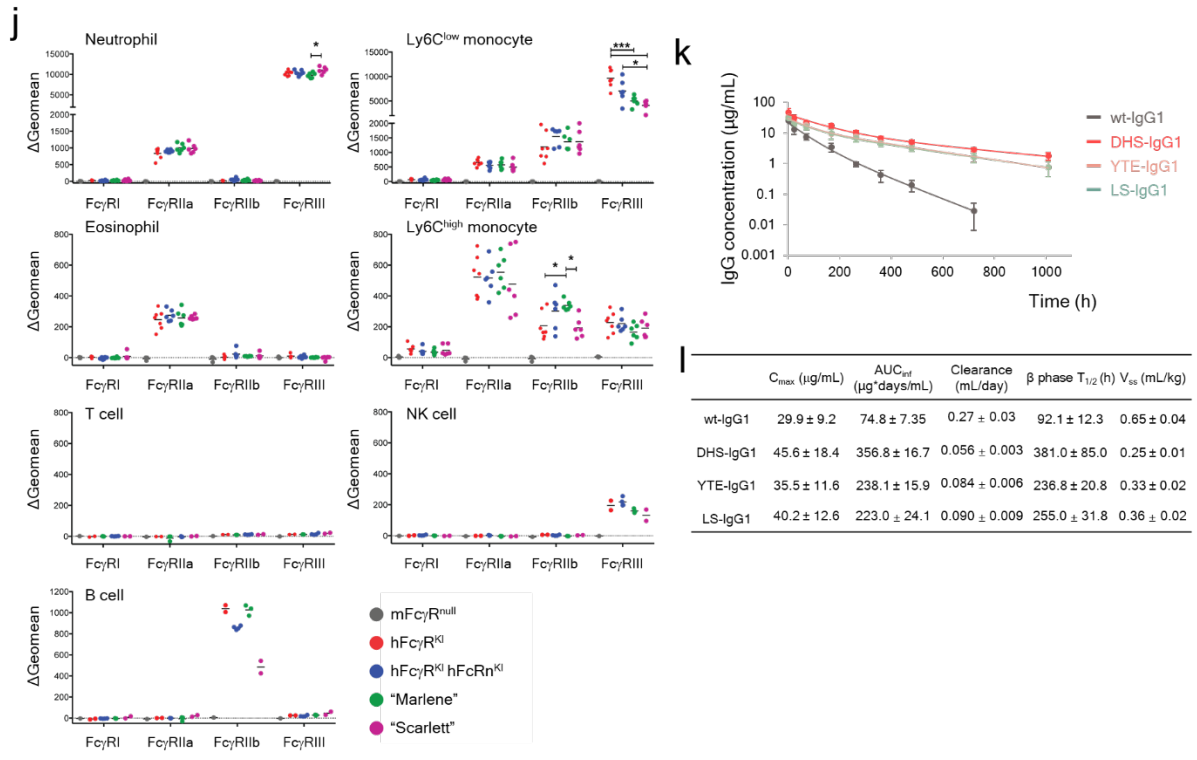

	C_{max} (μg/mL)	AUC_{inf} (μg*days/mL)	Clearance (mL/day)	β phase $T_{1/2}$ (h)	V_{ss} (mL/kg)
wt-IgG1	29.9 ± 9.2	74.8 ± 7.35	0.27 ± 0.03	92.1 ± 12.3	0.65 ± 0.04
DHS-IgG1	45.6 ± 18.4	356.8 ± 16.7	0.056 ± 0.003	381.0 ± 85.0	0.25 ± 0.01
YTE-IgG1	35.5 ± 11.6	238.1 ± 15.9	0.084 ± 0.006	236.8 ± 20.8	0.33 ± 0.02
LS-IgG1	40.2 ± 12.6	223.0 ± 24.1	0.090 ± 0.009	255.0 ± 31.8	0.36 ± 0.02

Figure 2. IgG pharmacokinetics in new knock-in mouse models. (**a-h**) Generation of knock-in mice for human FcγRs, FcRn, β2m, IgG1 heavy chain and kappa light chain constant regions: (**a**) humanization of the mouse low-affinity receptor locus; (**b**) humanization of the ectodomains of mouse FcγRI; (**c**) humanization of the ectodomains of mouse FcRn; (**d**) humanization of the mouse β2m gene (B2m); (**e**) breeding strategy to generate Marlene mice; (**f**) replacement of the switch μ region of the mouse heavy chain locus by the constant region of human IgG1 heavy chain (IGHG1); (**g**) humanization of the kappa light chain gene (IGK); (**h**) breeding strategy to generate Scarlett mice; (**a-d, f-g**) representations are not drawn to scale. Coordinates are based on mouse (GRCm38.p4) and human (GRCh38.p7) genomic assemblies; mouse genes are in empty rectangles, genomic coordinates are in black; human genes are in solid rectangles, genomic coordinates are in grey, black triangles represent LoxP sites. mb; exon encoding the transmembrane and intracytoplasmic domains; H; exon encoding the hinge domain. Neo; selection cassette. Mouse silhouette was created by co-author, Dr. Pierre Bruhns. (**i**) Immunohistochemical localization of hFcRn or mFcRn in tissue sections of human spleen, and spleen sections from of $hFc\gamma R^{KI}$ mice (VG1543 × VG6074) and Scarlett mice. Scale bar = 200 μm. **(j)** hFcγR expression on different cell populations from the spleen of $Fc\gamma R^{null}$ (negative control), $hFc\gamma R^{KI}$ (positive control), $hFcRn^{KI}$ $hFc\gamma R^{KI}$, Marlene and Scarlett mice. P-values by one-way Anova with Tukey's multiple comparison tests, * $P \leq 0.05$ and *** $P \leq 0.001$. (**k**) Change in serum IgG concentration following tail vein administration of 2 mg/kg of antibody in Scarlett ($hFcRn^{KI}$ $h\beta2m^{KI}$ $hFc\gamma R^{KI}$ hIgG1, κ^{KI}) mice (n=6). Data are presented as mean ± standard deviation.

a

K_D (μM)	FcγRI (x10^{-3})	FcγRIIa$_{H131}$	FcγRIIa$_{R131}$	FcγRIIb	FcγRIIIa$_{F158}$	FcγRIIIa$_{V158}$
wt-IgG1	0.21 ± 0.02	0.22 ± 0.06	1.16 ± 0.25	2.64 ± 0.39	1.17 ± 0.23	0.17 ± 0.04
DHS-IgG1	0.28 ± 0.02	0.27 ± 0.04	0.95 ± 0.02	2.91 ± 0.54	0.48 ± 0.07	0.18 ± 0.03
YTE-IgG	0.29 ± 0.02	0.62 ± 0.18	3.20 ± 0.26	6.24 ± 0.10	4.41 ± 0.93	0.82 ± 0.11
LS-IgG1	0.58 ± 0.12	0.41 ± 0.30	1.21 ± 0.02	2.25 ± 0.03	0.64 ± 0.09	0.52 ± 0.09

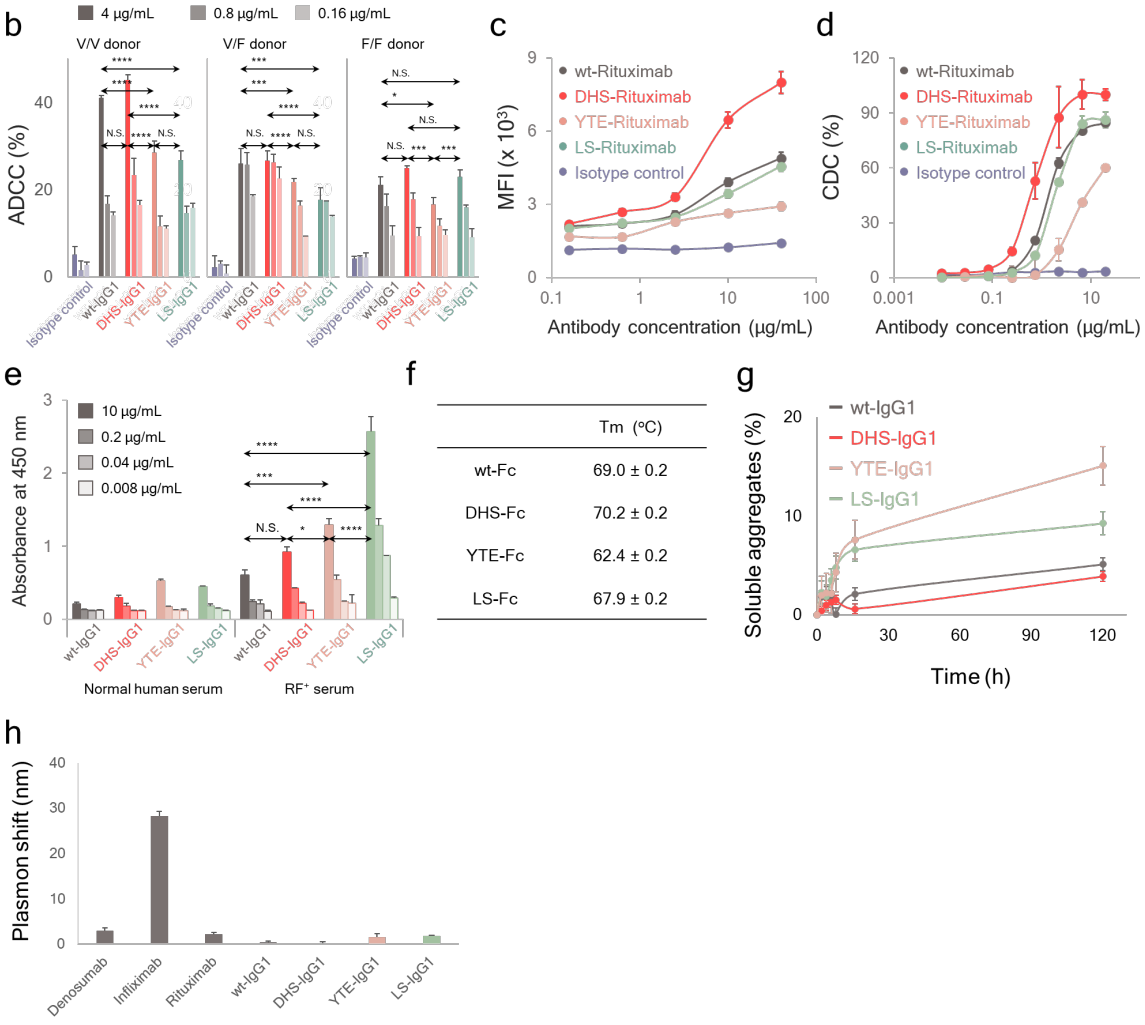

Figure 3. Features of DHS Fc variants relevant to therapeutic antibody development. (**a**) ADCC assay of SK-BR-3 with PBMCs from FcγRIIIa *V/V*, *V/F*, or *F/F* donors. (**b**) C1q deposition on CD20$^+$ Raji cells revealed by flow cytometry. (**c**) CDC assay of Rituximab-Fc variants with Raji cells as a function of antibody concentration. (**d**) Binding to rheumatoid factor (RF) measured by ELISA. P-values by two-way ANOVA test, N.S. P ≥ 0.05, * P ≤ 0.05, ** P ≤ 0.01, *** P ≤ 0.001 and **** P ≤ 0.0001. (**e**) Extent of antibody aggregation following thermal stress (50 ºC incubation) of Trastuzumab variants, measured by size exclusion chromatography (SEC). (**f**) Antibody self-association properties measured by affinity-capture self-interaction nanoparticle spectroscopy (AC-

882 SINS) assay. Data are from one experiment representative of three experiments using three individual
883 donors (**a**-**d**). Errors in all plots and tables represent standard deviations from triplicate experiments.

884

Table 1. K_D values for binding of DHS, YTE, LS variants or wt IgG1 to hFcRn:hβ2m dimer at pH 5.8 and 7.4.

K_D (nM)	pH 5.8	pH 7.4		
		Low density	Medium density	High density
wt-IgG1	550 ± 50	N.D.	N.D.	N.D.
DHS-IgG1	110 ± 20	N.D.	N.D.	N.D.
YTE-IgG1	23 ± 1	N.D.	4730 ± 480	4290 ± 310
LS-IgG1	55 ± 3	N.D.	946 ± 170	567 ± 152

All IgG variants analyzed with hFcRn:hβ2m dimer and their kinetic values were analyzed by the equivalent binding model. Data are presented as mean ± standard deviation from triplicate experiments.

Table 2. Pharmacokinetic parameters for hemizygotic Tg276 hFcRn transgenic mice.

	$AUC_{inf.}$ (μg*days/mL)	Clearance (mL/day)	β phase $T_{1/2}$ (h)	V_{ss} (mL/kg)
wt-IgG1	30.0 ± 1.6	0.66 ± 0.17	49.6 ± 13.4	1.50 ± 0.15
DHS-IgG1	157.9 ± 3.4	0.11 ± 0.01	290.9 ± 25.6	0.59 ± 0.11
YTE-IgG1	96.9 ± 3.3	0.24 ± 0.03	148.4 ± 36.8	0.72 ± 0.14
LS-IgG1	84.4 ± 2.0	0.21 ± 0.03	92.9 ± 6.1	0.60 ± 0.06

Data are presented as mean ± standard deviation (n=11).

Table 3. Pharmacokinetic parameters for Scarlett ($hFcRn^{KI}$ $h\beta2m^{KI}$ $hFc\gamma R^{KI}$ hIgG1, κ^{KI}) mice

	C_{max} (mg/mL)	AUC_{inf} (μg*days/mL)	Clearance (mL/day)	β phase $T_{1/2}$ (h)	V_{ss} (mL/kg)
wt-IgG1	29.9 ± 9.2	74.8 ± 7.35	0.27 ± 0.03	92.1 ± 12.3	0.65 ± 0.04
DHS-IgG1	45.6 ± 18.4	356.8 ± 16.7	0.056 ± 0.003	381.0 ± 85.0	0.25 ± 0.01
YTE-IgG1	35.5 ± 11.6	238.1 ± 15.9	0.084 ± 0.006	236.8 ± 20.8	0.33 ± 0.02
LS-IgG1	40.2 ± 12.6	223.0 ± 24.1	0.090 ± 0.009	255.0 ± 31.8	0.36 ± 0.02

Data are presented as mean ± standard deviation (n=6).

Table 4. K_D values for human FcγRs determined by SPR.

K_D (μM)	FcγRI (x10^{-3})	FcγRIIa$_{H131}$	FcγRIIa$_{R131}$	FcγRIIb	FcγRIIIa$_{F158}$	FcγRIIIa$_{V158}$
wt-IgG1	0.21 ± 0.02	0.22 ± 0.06	1.16 ± 0.25	2.64 ± 0.39	1.17 ± 0.23	0.17 ± 0.04
DHS-IgG1	0.28 ± 0.02	0.27 ± 0.04	0.95 ± 0.02	2.91 ± 0.54	0.48 ± 0.07	0.18 ± 0.03
YTE-IgG	0.29 ± 0.02	0.62 ± 0.18	3.20 ± 0.26	6.24 ± 0.10	4.41 ± 0.93	0.82 ± 0.11
LS-IgG1	0.58 ± 0.12	0.41 ± 0.30	1.21 ± 0.02	2.25 ± 0.03	0.64 ± 0.09	0.52 ± 0.09

All IgG variants analyzed with monomeric Fc receptors and their kinetic values were analyzed by the equivalent binding model. Data are presented as mean ± standard deviation from triplicate experiments.

Table 5. Tm measurement by Differential Scanning Fluorimetry (DSF).

	Tm (^{o}C)
wt-Fc	69.0 ± 0.2
DHS-Fc	70.2 ± 0.2
YTE-Fc	62.4 ± 0.2
LS-Fc	67.9 ± 0.2

Data are presented as mean ± standard deviation (n=3).